Electron energization with bursty bulk flows: MHD with Embedded Particle-in-Cell Simulation

Xiantong Wang[1], Shasha Zou[1], Zihan Wang[2], Weijie Sun[3], Yuxi Chen[4], Gábor Tóth[1]

[1]Department of Climate and Space Sciences and Engineering, University of Michigan, Ann Arbor, MI, USA
[2]Department of Physics, University of Texas at Arlington, Arlington, TX, USA
[3]Space Science Laboratory, University of California, Berkeley, CA, USA
[4]Center for Space Physics and Department of Astronomy, Boston University, Boston, MA, USA

Key Points:

- For the first time, we simulate the bursty bulk flow events with kinetic physics embedded in a global magnetosphere model.
- The electron velocity distributions demonstrate different anisotropy features at different locations surrounding the BBF.
- Energy dependent electron pitch angle distribution evolutions are identified in the simulation.

Corresponding author: Xiantong Wang, xtwang@umich.edu

Abstract

Using the two-way coupled magnetohydrodynamics (MHD) withembedded kinetic physics model, we perform a substorm event simulation to study the electron energization phenomena in Bursty Bulk Flow (BBF) events. The simulation results along a Magnetospheric Multiscale (MMS) satellite trajectory show good agreement with observations. Detailed simulation results of a 4-minute interval show the electron velocity distribution functions (VDFs) evolution during BBFs. The electrons exhibit significant energization after the arrival of the BBF. More specifically, when the dipolarization front is near $-15\,R_E$, electrons from the rear end of the BBF to the flux pileup region (FPR) of the BBF demonstrate significant energization. We track the pitch angle distributions (PADs) for electrons at the FPR following the propagation of the BBF. The PADs for electrons show energy dependent features: lower energy electrons exhibit "two-hump" PAD and higher energy electrons demonstrate "pancake" distribution indicating the betatron acceleration mechanism at the FPR.

Plain Language Summary

Bursty bulk flows (BBFs) are identified as the fast earthward-propagating flows from magnetic reconnection in Earth's magnetotail. BBFs are related to particle energization process reported by satellite observations. For the first time, we use a novel numerical model that simulates kinetic physics directly in a global model. The energization of the electrons associated with BBF is demonstrated by the model. The electron velocity distribution functions (VDFs) extracted from multiple locations associated with BBF demonstrate good agreements with the observations. The energy-dependent electron pitch angle distribution at the leading part of the BBF can be explained by the enhancement of the local magnetic field.

1 Introduction

Initially observed by Baumjohann et al. (1990) and later further demonstrated by Angelopoulos et al. (1992, 1994a) using AMPTE satellite data, bursty bulk flows (BBFs) are characterized by their transient ($\sim$ 10-minute) fast ($\sim$ 400 km/s) plasma flow enhancement in the magnetotail. Concurrently, an increased intensity in the B_z component of the magnetic field is typically identified at the dipolarization fronts (DFs) during these BBF events (Nakamura et al., 2002; Runov et al., 2009; Fu et al., 2012). These DFs arise from magnetic reconnection sites within the magnetotail and propagate earthward simultaneously with the BBFs. Consequently, BBFs serve as an efficient mechanism for transporting magnetic flux from the magnetotail to the inner magnetosphere (Angelopoulos et al., 2013; Huang et al., 2015; Nakamura et al., 2009). Furthermore, BBFs are associated with plasma phenomena, such as plasma wave activities, the injection of energetic particles into the inner magnetosphere and field-aligned currents and particle precipitations into the ionosphere (Henderson et al., 1998; Angelopoulos et al., 1996; Gabrielse et al., 2014; Angelopoulos et al., 1997).

Numerical simulations have played a pivotal role in the study of BBFs within the magnetotail over the past several decades. Birn et al. (1996) utilized regional magnetohydrodynamic (MHD) simulations to demonstrate the connection between the plasmoid formation and dipolarization in the inner magnetosphere. In subsequent simulation work by Birn et al. (2004), the authors discovered that the reduction of the flux tube entropy is facilitating the earthward propagation of the BBFs. In addition to the regional MHD simulations for the magnetotail, the development of global MHD models enables the study of the BBFs in a more realist setup. Employing the Lyon-Fedder-Mobarry (LFM) global MHD magnetosphere model (Lyon et al., 2004), Wiltberger et al. (2000) simulated several fast flow channels in the magnetotail during an isolated subtorm, and the plasma and magnetic field properties showed good agreement with the observation reported by

Angelopoulos et al. (1992). The OpenGGCM model (Raeder et al., 2008) was also used by Ge et al. (2011) to study the propagation of the dipolarization front and they concluded the causality between the auroral breakup represented by the simulated energy flux in the simulation and the flow vortices formed around the BBF flows. Recent investigations using numerical simulation have further advanced the understanding of BBF events. Wiltberger et al. (2015) conducted a high-resolution global MHD simulation with the LFM model to study the BBF behaviour under steady southward IMF conditions. The authors confirmed that BBFs are driven by the onset of new reconnection and its related fast earthward flows. Superposed epoch analysis was also conducted, and the overall plasma and magnetic field properties were found to be similar to the observations although with differences in plasma density profiles near the BBFs (Wiltberger et al., 2015).

Despite the progress made with regional and global MHD simulations on the general properties of the BBF events as described above, there is a need to simulate BBFs with kinetic models to investigate the particle velocity distribution evolution and energization processes. First, the acceleration near the neutral line at the site of reconnection was investigated. In these studies, energetic electrons up to approximately 300 keV near the center of the diffusion region were observed by the Wind spacecraft (Øieroset et al., 2002). The energization mechanism of these relativistic electrons were later examined by regional particle-in-cell simulations. The electrons with velocity component $V_x \sim 0$ at the X line are accelerated across the tail by the inductive reconnection electric field E_y (Hoshino, 2005; Pritchett, 2006). Subsequently, betatron acceleration related to the magnetic field dipolarization when the plasma flow propagates towards Earth was studied to explain the electron acceleration signature during substorms (Baker et al., 1982; Birn et al., 1998; Asano et al., 2010). Meanwhile, the energization mechanism of ions was also studied by observations and simulations. Using THEMIS observations, X.-Z. Zhou et al. (2010) noticed that energetic ions exist ahead of the DF, which was later explained by precursor flow formed by ion reflections using test-particle simulation (X.-Z. Zhou et al., 2011). This argument is also supported by implicit PIC simulations (Eastwood et al., 2015). This ion reflection also exists in tailward DFs from ARTEMIS observations (X.-Z. Zhou et al., 2015). Similar to electrons, Betatron and Fermi accelerations are also found to account for ion energization (Runov et al., 2015; X.-Z. Zhou et al., 2019; Lu et al., 2016; Xu et al., 2019). In addition to velocity distribution functions, understanding the particle pitch angle distribution (PAD), especially the electron PAD, is crucial for comprehending particle energization associated with BBFs. Various electron PADs have been observed in the wake of DFs. Among them, the pancake distribution (electron pitch angle primarily at 90°) has been reported within the evolving Flux Pileup Regions (FPRs) (Fu et al., 2011; C. Liu et al., 2017) near the neutral sheet, and it is recognized as being associated with the betatron acceleration mechanism (Fu et al., 2011). However, the detailed information regarding when and where particles become energized and how their velocity or pitch angle distribution functions are altered while the BBF structure evolves remains an open question.

Currently, MHD models are unable to capture the kinetic physics of the plasma, and the PIC simulations mentioned earlier are limited to regional simulations without a global magnetosphere configuration. As a result, there remains a significant gap in the literature regarding self-consistent simulations that couple global MHD and localized PIC models to investigate the evolution of BBF events. In this paper, we will use the two-way coupled MHD and PIC modeling approach to fill in this gap. A substorm event on May 16, 2017 is simulated by the BATSRUS MHD model with local kinetic physics captured by the FLEKS PIC code. This two-way coupled model allows the investigation of the evolution of electron velocity distributions and the subsequent formation of anisotropy at various locations of the BBF. The pitch angle distributions of the electrons can also be examined to provide insights into the field-aligned current generation process.

The model description and simulation setup are described in Section 2, the simulation results are presented in Section 3 and we conclude in Section 4.

2 Simulation Setup

We use MHD with embedded PIC (MHD-EPIC) model (Daldorff et al., 2014; Chen & Tóth, 2019) to simulate Earth's magnetosphere. In MHD-EPIC, the BATS-R-US MHD code (Powell et al., 1999; Tóth et al., 2008) and semi-implicit particle-in-cell (PIC) code FLEKS (Chen et al., 2023) are two-way coupled through SWMF (Tóth et al., 2012; Gombosi et al., 2021). A three-dimensional block-adaptive Cartesian grid of BATS-R-US is used to cover the entire computational domain: $-224\,R_E < x < 32\,R_E$ and $-128\,R_E < y, z < 128\,R_E$ in GSM coordinates. The semi-relativistic ideal MHD with electron pressure equations are solved in most of the simulation domain. The PIC model is solved in a box region with a spherical cut out. The box is in the magnetotail ($-60\,R_E < x < 0$ and $-12\,R_E < y, z < 12\,R_E$) from which the sphere with radius $r = 10\,R_E$ centered around Earth is excluded to avoid overlap with the Rice Convection Model (RCM)(Wolf et al., 1982; Toffoletto et al., 2003) simulating the inner-magnetosphere. Moreover, we solve the Hall MHD equations around the PIC region ($-100\,R_E < x < 0$, $-30\,R_E < y < 30\,R_E$, and $-20\,R_E < z < 20\,R_E$ excluding a sphere with radius $r = 3\,R_E$ centered around Earth) to achieve more consistent coupling. The grid resolution is set to $1/8\,R_E$ for both the PIC and MHD models in the PIC region. The ionospheric electrodynamics is simulated by the Ridley Ionosphere Model (RIM) (Ridley et al., 2004), which solves a Poisson-type equation for the electric potential on a 2-D spherical grid with a $1^\circ \times 1^\circ$ grid resolution. The MHD-EPIC model has been applied to studying several planetary and moon magnetospheres, including Mercury (Chen et al., 2019; Li et al., 2023), Earth (Chen et al., 2017, 2020; Wang et al., 2022a, 2022b), Mars (Ma et al., 2018), and Ganymede (Tóth et al., 2016; H. Zhou et al., 2019, 2020).

In PIC simulations, reduced speed of light c and ion-electron mass ratio m_i/m_e are often used to make the simulation feasible to the computational resources (Lapenta et al., 2010; Daughton et al., 2011; Y.-H. Liu et al., 2014). In the presented simulation, c = 10,000 km/s to accelerate the convergence of the implicit electric field solver, and m_i/m_e = 100 to increase the electron kinetic scale. The ion and electron masses per charge are also increased by a factor of 16 to increase the kinetic scales (ion inertial length and electron skin depth) so that they can be resolved with an affordable grid resolution. Tóth et al. (2017) concludes that by introducing this scaling factor 16, (a) the solution of the equations is not sensitive to the scaling at global scales, and (b) the solutions at the kinetic scale, such as the width of the ion diffusion region and the overall structures of the reconnection jets, are proportional to the scaling factor but otherwise remain the same. In our simulation, the ion inertial length in most areas of the magnetotail is larger than $1\,R_E$ with the scaling factor applied, which can be well resolved by the $1/8\,R_E$ grid resolution. The electron skin depth is 10 times smaller, which is only marginally resolved, but the solution overall remains valid at the resolved scales (Chen & Tóth, 2019).

We apply the MHD-EPIC model to the substorm event on 16 May 2017 from 11:00:00 to 15:00:00 UT. Panel 1(a) shows the 3-D overview of the simulation domain at T = 13:30:00 UT from the simulation presented in this paper. The gray isosurface marks the simulation domain that is covered by the kinetic model while the rest of the simulation domain is simulated using MHD. The color contour in panel (a) is the plasma bulk velocity in the x direction on the equatorial plane, and the semi-transparent box shows the region where the PIC model is applied. The $r = 3\,R_E$ body is also visualized colored with the radial component of the current density j_r. A closer look at the $r = 3\,R_E$ body is placed at the lower right corner. First, the BATS-R-US and RIM models are run to reach a quasi-steady state under the solar wind condition at 11:00:00 using local time stepping with 2,500 iterations. Next, the FLEKS and RCM models are switched on and the SWMF is run in time-accurate mode. The most relevant solar wind parameters, in-

cluding the solar wind density ρ, velocity V_x and IMF B_z, are plotted in Panel 1(c), suggesting moderate driving condition. This substorm was observed in the auroral electrojet index (AE), presented in Panel 1(c), and also by individual ground magnetometers near Alaska (not shown). The MMS observations also captured the loading and the subsequent unloading processes, which initiated at 13:21 UT. The subtorm onset based on the AE index is later than the MMS observation and at about 13:42 UT.

3 Results

3.1 Overview of the substorm

Throughout the simulated event, the MMS1 satellite traversed the dawn side of the magnetotail with an averaged location at $(-14.23, -8.99, 0.37)\, R_E$ in GSM coordinates. As depicted in Figure 1(b), we present the profiles of the total magnetic field strength (B_t), its x and z components, and the x component of the plasma bulk velocity in GSM coordinates from MMS measurements (in black) and the simulation outputs (in red). The persistently negative x component of the magnetic field shows that the virtual satellite position is on the same side as the MMS satellite in the tail current sheet. From the MMS observation, loading and unloading processes can be seen clearly in the variation of the total magnetic field strength. The decline of B_t commenced around 13:20 UT and signaled the unloading process. This trend is not captured by the MHD-EPIC model, because the simulated magnetotail is constantly volatile in this time range. This can also be observed from the B_z and V_x comparisons. The MMS observation shows a dipolarization between 13:45 UT to 14:00 UT, which is also captured by the MHD-EPIC model. Multiple earthward flows are evident within the ion bulk velocity V_x, attaining maximum speeds exceeding 500 km/s. Although it is difficult to have one to one match for each dipolarization, the overall magnitudes of the B_z and V_x exhibit reasonable agreement between the observation and simulation during the dynamic time in the magnetotail. Illustrated in Figure 1(a) is the comprehensive layout of the simulation domain, revealing the ion bulk velocity contour on the equatorial plane, with peak speeds surpassing 700 km/s. Multiple instances of earthward flow injections manifest on the equatorial plane, suggesting that the simulation successfully captures multiple earthward plasma flows with the MHD-EPIC model.

In the following subsections, we will take a closer look at the detailed structure of the BBF and the associated particle velocity distribution functions at multiple locations surrounding the BBF.

3.2 General properties of the BBF

The observations in Figure 1(b) show that the magnetotail became more active after $t \approx$13:20 UT, when the unloading process initiated. Figure 3 (a)-(d) show a four-minute time interval from 13:49 UT to 13:52 UT of a major simulated BBF event identified by the peak in V_x in Figure 1(b), obtained from the simulated PIC region. To analyze the BBF characteristics on the current sheet better, the physical quantities are extracted on the surface where $B_x = 0$. The z component of the magnetic field B_z in GSM coordinate is plotted on the current sheet surface with color in each panel. The red contour lines delineate areas where the earthward ion bulk velocity V_x is larger than 400 km/s. The targeted BBF can be identified as the rapid flow channels propagating towards Earth on the dawn side. At the front of these earthward flow channels, there are enhancements in B_z, i.e. dipolarization fronts. The B_z enhancement initiated at $x \approx -20\,\mathrm{R_E}$ and propagated into the inner-magnetosphere in the subsequent minutes. Compared to the background B_z, which is less than 10 nT in most of the magnetotail, at the DF, B_z is enhanced above 30 nT. The simulated spatial scale of the DF is about $3\,\mathrm{R_E}$ at the early stage of the BBF and expanded to $\approx 5\,\mathrm{R_E}$ as it propagates closer to Earth, consistent with the statistical analysis of bursty bulk flow events Angelopoulos et al. (1994b).

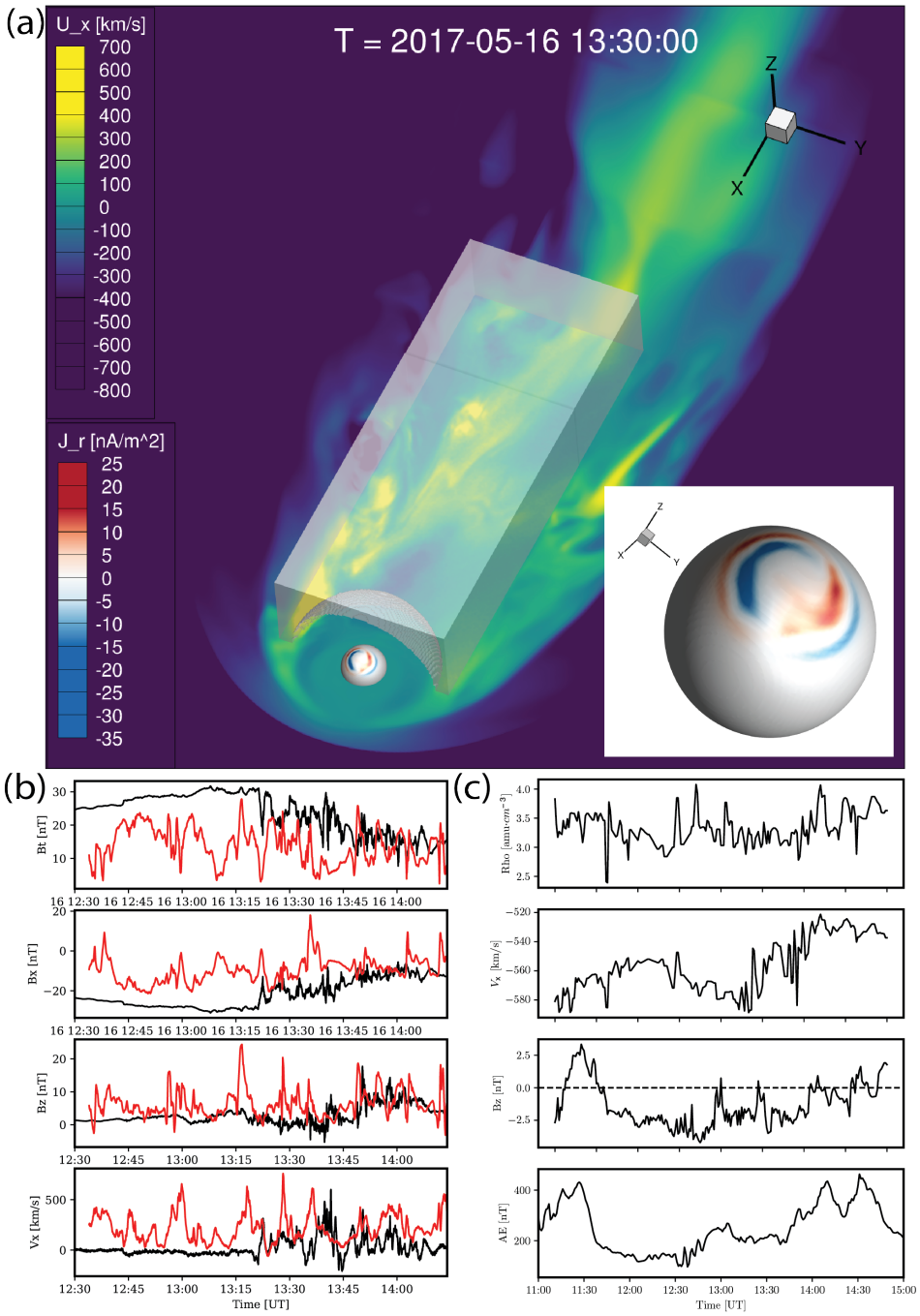

Figure 1. (a) Overview of the simulation domain. The color contour of the x direction of the plasma bulk velocity is plotted on the equatorial plane at 2017-05-16 13:30 UT. The area inside the gray iso-surface is simulated by the PIC model and the rest of the simulation domain is simulated by the MHD model. The radial current is plotted on the $R = 3\,R_E$ surface. (b) Comparison between the simulation output (red) and the MMS observations (black). (c) Key solar wind parameters used as drivers and the observed AE index.

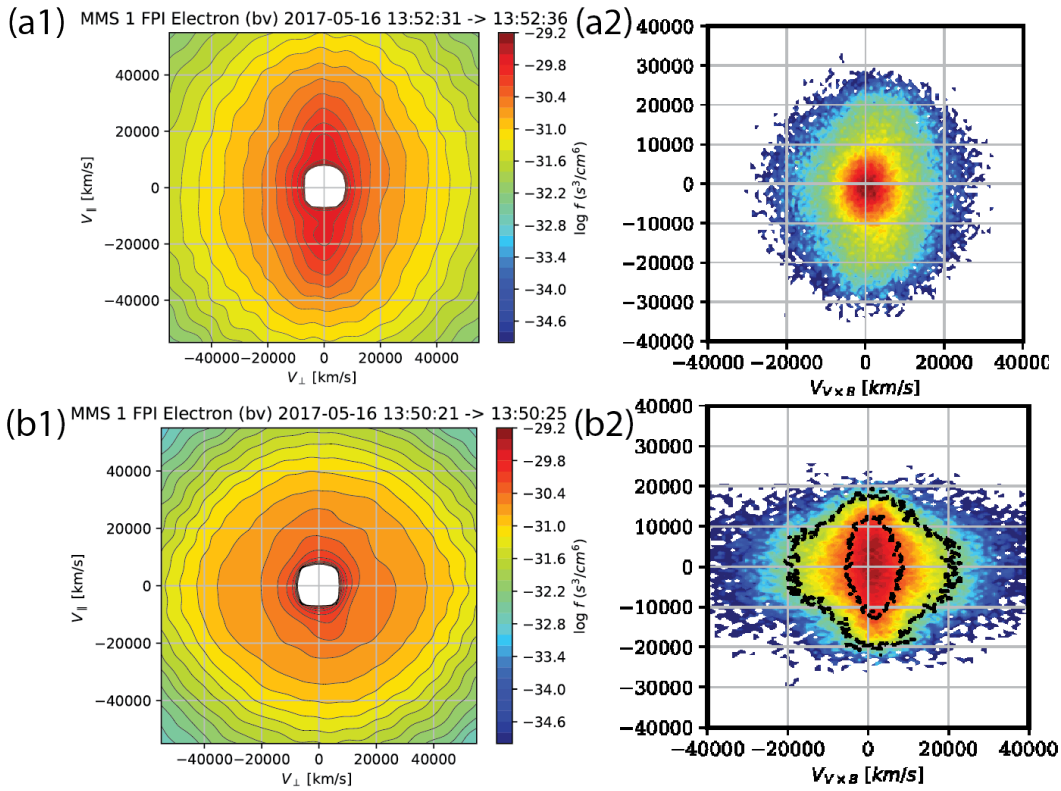

Figure 2. Electron velocity distribution function comparison between MMS (a1, b1) and simulation (a2, b2)). (a1, a2) Electron VDFs at the tailing part of the BBF. (b1, b2) Electron VDFs near the B_z maximum of the BBF.

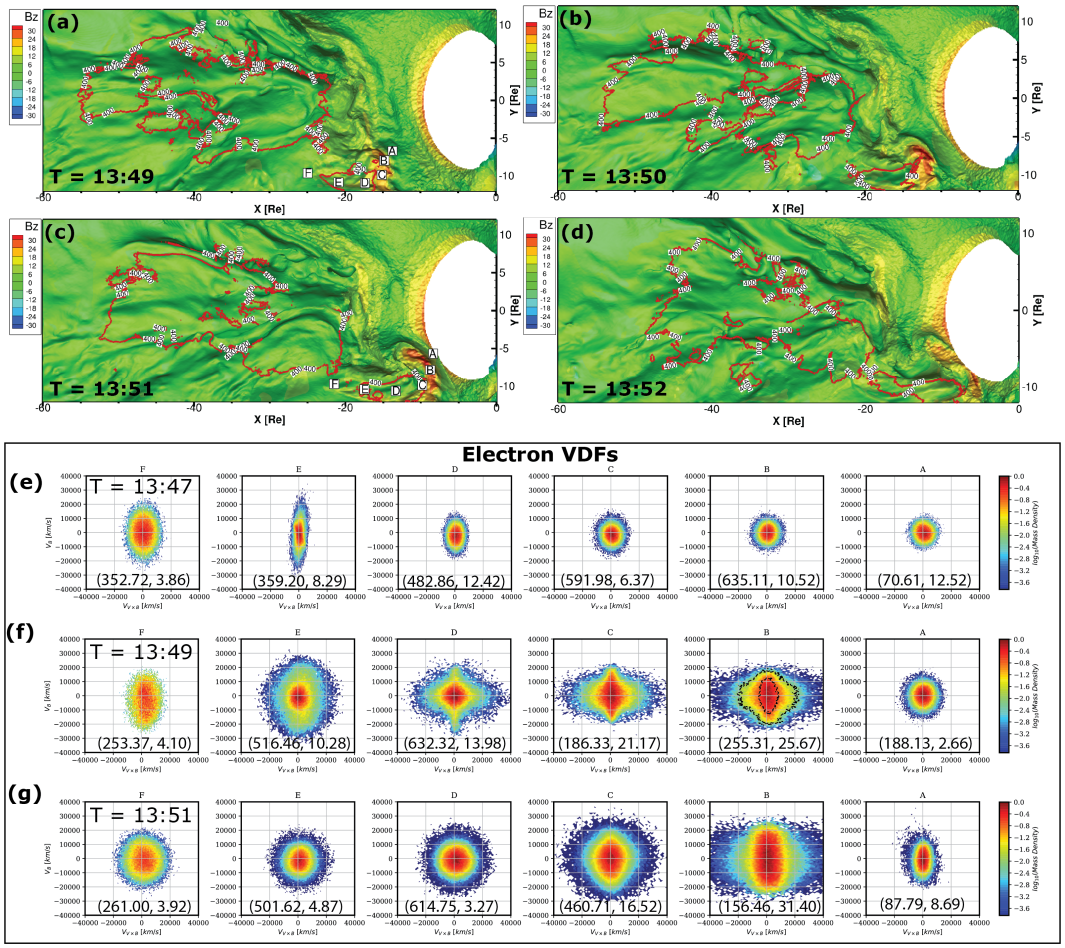

Figure 3. (a)-(d) The $B_x = 0$ iso-surface colored by B_z at four times from 13:49 UT to 13:52 UT. The 400 km/s contour lines of the plasma bulk velocity in the x direction are shown in red. (e)-(f) The electron velocity distribution functions (VDFs) at locations A to F annotated in Panel (a). (g) The electron VDFs at the time and locations A to F annotated in Panel (c). The pair of numbers in parentheses in Panels (e)-(g) show the ion bulk velocity V_{ix} (in km/s) and the magnetic field component B_z (in nT).

3.3 Electron velocity distributions evolution around the BBF

To further investigate the electron energization process associated with the BBF, the electron VDFs observed from the Fast Plasma Investigation (FPI) suite from MMS satellite (Pollock et al., 2016) are presented in Figure 2. Panel (a1) is extracted inside the trailing part of the BBF while panel (b1) is extracted near the B_z maximum of the BBF. The corresponding electron VDFs from the MHD-EPIC model are presented in panels (a2) and (b2), respectively. At the trailing part of the BBF, the electron VDF demonstrates dominantly parallel anisotropy, indicating that the electrons are experiencing Fermi acceleration. At the leading part of the BBF near the B_z maximum, the high energy electrons are energized favorably in the perpendicular directions, indicating the betatron acceleration mechanism, while the low energy electrons still exhibit parallel anisotropy. The agreements confirm a distinction in the energization mechanisms between the leading and trailing parts of the BBF, which is also reported by Sun et al. (2022).

To analyze the electron velocity distributions in more detail, six specific sampling locations, labeled from A to F, have been chosen to extract velocity distribution functions for examination and are annotated in Panels (a) and (c) of Figure 3. These points were selected based on their relative positions with respect to the general BBF structure, spanning from the far end of the BBF to the immediate location in front of dipolarization front. Specifically, F is positioned beyond the rear end of the BBF, while E is within the BBF and closer to the rear end. Moving closer to Earth, D marks the location in the middle of the fast flow area. C is situated nearer to the dipolarization front, while B precisely coincides with the DF where the magnetic field B_z component reaches its maximum. Finally, A is situated ahead of the DF, offering insight into the plasma environment preceding the BBF within the near-Earth plasma sheet. Panels (e) to (g) illustrate electron velocity distribution functions extracted from the aforementioned sampling sites. These velocity distributions are projected onto the perpendicular (x-axis) and parallel (y-axis) directions relative to the local magnetic field direction. The perpendicular direction follows the orientation of $V \times B$, with V representing the local ion bulk velocity. The local ion bulk velocity has been subtracted from the particle velocities. The local ion bulk velocity and B_z at those sampling locations from three time points are annotated in Panels (e)-(g) in Figure 3.

First, we examine the perturbations due to the incoming BBF by extracting the electron VDFs at the same locations for 13:47 UT (panel e) and 13:49 UT (panel f). The local magnetic field is updated accordingly at each cadence to project the particle velocities onto the coordinate system presented. At locations F and E, electrons exhibit strong velocity anisotropy in the parallel direction, i.e., cigar shape, indicating Fermi accelerations. This feature is transient and disappears atlocation E after 2 minutes. At locations B, by comparing Panel (e) and (f), prominent energization and heating can be identified by the expanded VDFs in both perpendicular and parallel directions. Thus, the comparison between the solutions at 13:47 UT and 13:49 UT clearly shows that the propagating BBF can significantly perturb the local electron VDFs.

Second, we examine electron VDFs at different locations across the BBF structure at 13:49 UT in panel (f) of Figure 3. At location F, electrons start with parallel anisotropy, due to being in close vicinity of the reconnection site. At location E, the perpendicular energy of electrons is slightly enhanced. Advanced to location D, the perpendicular electron energy is enhanced substantially, altering the VDF to become perpendicularly dominant. This indicates that electrons are sensitive to the betatron acceleration mechanism. From location C to B, electrons with different energies show different evolution. Higher energy electrons experience substantial energization in the perpendicular direction influenced by the betatron acceleration mechanism, while electrons at lower energies clearly prefer parallel direction suggesting the dominant role of Fermi acceleration. Moreover,

the electrons in front of the DF at location A exhibit a significantly lower temperature than those at the DF.

Third, we compare electron VDFs at similar relative locations of the BBF following its earthward propagation. Panel (f) presents the electron VDFs during the early phase of the BBF at 13:49 UT, while the corresponding VDFs at 13:51 UT are illustrated in Panel (g). By comparing the corresponding panels at these two time cadences, one can see that the electron VDFs are more isotropic behind the DF at locations E and D. At locations C and B, which are closer to the strengthened DF, the electron VDFs show continuing energizations and heating. At 13:51 UT, the local B_z enhanced to 31.40 nT at location B from 25.67 nT at 13:49 UT, which results in more prominent betatron acceleration that can be identified from the VDF. The different anisotropy trends for low and high energy electrons persist while the BBF evolves.

3.4 Electron pitch angle distributions associated with the BBF

In Figure 4, we present the electron (a1-a3) PADs as a function of energy at 13:49 UT, 13:50 UT, and 13:51 UT. Note that these particles are extracted at the location where B_z reaches its maximum value of the Flux Pileup Region (FPR). The electron PADs exhibit distinct energy-dependent evolutions. To closely analyze this field-aligned PAD, electrons are divided into two energy groups: low ($0.5 - 2.2$ keV) and high energy ($>$ 2.2 keV). At 13:49 UT, when the peak FPR is situated at around $-14.8\,R_E$, high-energy electrons display a pancake PAD. As the FPR propagates closer to Earth at $-11.9\,R_E$ at 13:50 UT and at $-8.4\,R_E$ at 13:51 UT, the pancake PAD for the high-energy electrons remains prominent, as evident in Panel (b2). However, the peak flattens and the distribution becomes slightly more isotropic. This suggests that betatron acceleration dominates the process. On the other hand, for low energy electrons the PAD transitions from a pancake-like PAD to a butterfly distribution with maxima around 30° and 150°), suggesting that the Fermi acceleration mechanism plays a more significant role for electrons in this energy range. The specificity of the electron PAD over energy bands was also discovered by a THEMIS D observation by Runov et al. (2012) (Figure 9g): PAD in the higher energy band shows enhancement in 90° electron flux while the lower energy band demonstrate a "two-hump" distribution.

The preference for electron acceleration through betatron acceleration can be attributed to the nature of the increase of the magnetic field B_z in the presented FPR. In Figure 4(c), we illustrate the ion bulk velocity and B_z profiles of the FPR at 13:49 UT, 13:50 UT and 13:51 UT. Vertical lines indicate the locations where particles were extracted for the pitch angle analysis. The compression of the magnetic field is evident from the increased B_z peak from $\sim$25 nT to $\sim$33 nT, and reduced spatial expansion along the x direction. Both B_z peaks are situated within the lower ion bulk velocity region, with the second peak closer to the enhanced ion bulk velocity. This suggests that the rear part of the FPR is converging with the front, subsequently leading to betatron acceleration of electrons.

4 Conclusion

In this paper, we use the MHD-EPIC model to study electron distribution funciton evolution associated with BBFs in the magnetotail. A substorm event from 2017-05-16 11:00 UT to 15:00 UT is simulated by the numerical model. Different from prior simulation studies on BBF events, the magnetotail dynamics is simulated with kinetic physics, while the global magnetosphere configuration is simulated by the MHD model. Hence, the kinetic physics is simulated in a self-consistent manner throughout the substorm event. To demonstrate the kinetic features associated with the BBF events, the velocity and the pitch angle distributions of electrons are analyzed.

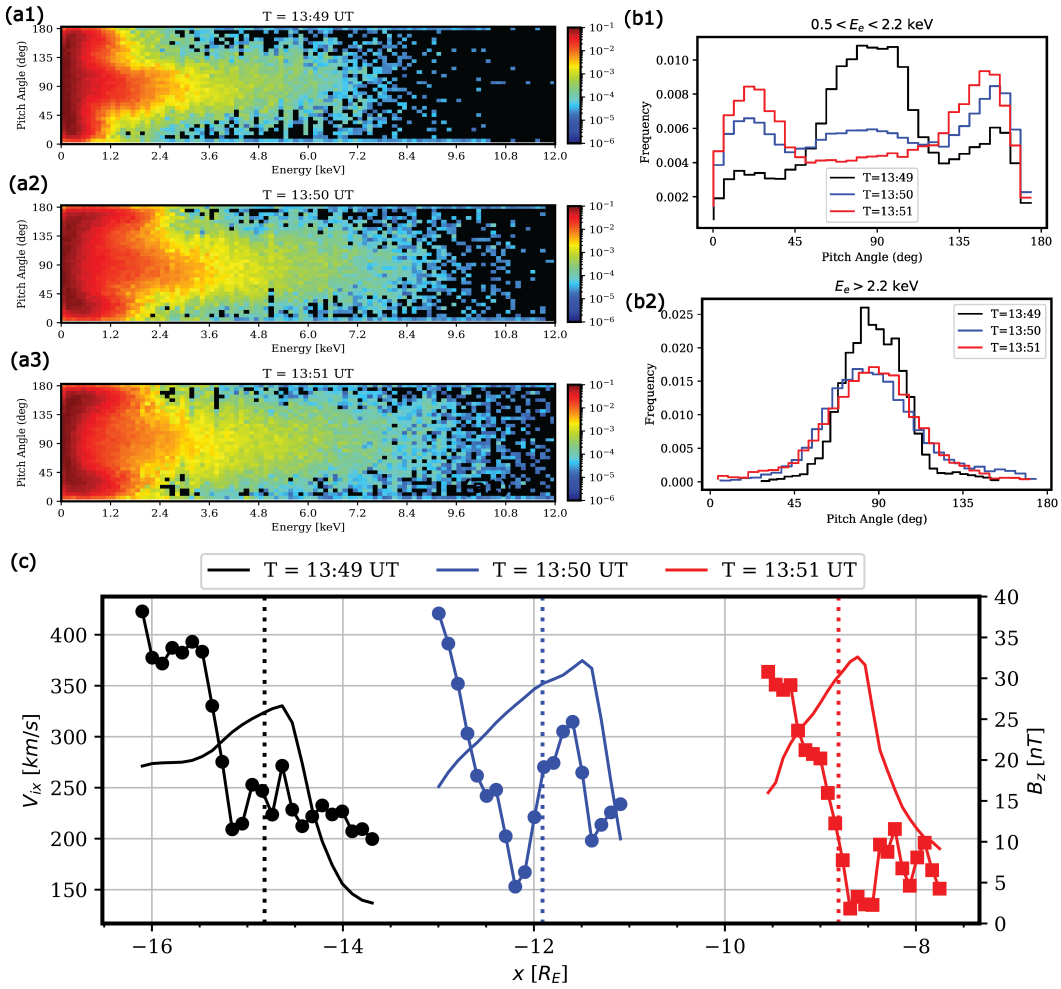

Figure 4. The pitch angle distribution functions from the B_z maximum at t = 13:49 UT, t = 13:50 UT and t = 13:51 UT. (a1)-(a3) The electron pitch angle distributions with regard to electron energy. (b1)-(b2) The pitch angle distributions for low energy (0.5 - 2.2 keV) and high energy (> 2.2 keV) electrons. (c) The ion bulk velocity and B_z profiles for the presented FPR at three different times.

We compare the magnetic field and plasma properties between the extracted virtual satellite locations and the MMS observation. The comparison yields good agreement, which indicates that the overall magnetosphere configuration is well reproduced by the MHD-EPIC model. We extract the electron energy distribution at the virtual satellite location, and find that the enhancement of energetic ($> 1\,\mathrm{keV}$) electron population coincides with the occurrance of the earthward fast flows, which indicates the correlation between the BBF events and the electron energization. A case study for a 4-minute time interval from 13:49 UT to 13:52 UT is performed to demonstrate the kinetic features associated with the BBF. The magnetic field component B_z at the DF is enhanced to above $30\,nT$ that agrees well with observations. The spatial scale of the dipolarization front (DF) from the simulation is observed to be $\approx 3\,R_E$, which also agrees with statistical satellite observations. Hence, the morphological feature of the BBF is well reproduced by the MHD-EPIC model. We compare the electron VDFs at the same location before and after the DF arrival. For electrons, the energization is significant in both perpendicular and parallel directions. By examining the VDFs at multiple locations inside the BBF, a clear trend of energization can be identified from the rear end of the BBF to the DF. Moreover, when the BBF is propagating closer to Earth, electrons with lower energy have more field-aligned velocities. We analyzed the electron PADs near the flux pileup region (FPR). The electron PADs evolutions show dependency on the energy bands. For low energy electrons (0.5 - 2.2 keV in the simulation), the PAD demonstrates "two-hump" distribution while for high energy electrons (> 2.2 keV in the simulation), pancake distribution is observed that is associated with betatron acceleration mechanism.

After identifying the energized electrons through velocity distribution functions and inferring the energization mechanism by examining the pitch angle distributions, there are still open questions regarding to energization of particles associated with BBFs, for example the source of the energized particles and the possible different energization processes for electrons with different initial energy and location. We aim to conduct investigations on these problems in the future using the two-way coupled MHD-EPIC model with particle tracking feature included.

Open Research

- The simulation output and scripts used for generating figures in this paper can be obtained online (https://doi.org/10.7302/61te-2903) through the University of Michigan's Deep Blue Data repository.
- The SWMF code (including BATS-R-US and FLEKS) is publicly available through the website (https://clasp.engin.umich.edu/research/theory-computational-methods/swmf-downloadable-software/).
- The MMS observational data is obtained through PySPEDAS. (https://doi.org/10.1007/s11214-018-0576-4).

Acknowledgments

This work was primarily supported by grant NASA 80NSSC20K1313. G. Toth acknowleges the support from NSF PRE-EVENTS grant No. 1663800. We acknowledge NASA Pleiades supercomputer for providing HPC and storage resources..

References

Angelopoulos, V., Baumjohann, W., Kennel, C., Coroniti, F. V., Kivelson, M., Pellat, R., ... Paschmann, G. (1992). Bursty bulk flows in the inner central plasma sheet. *Journal of Geophysical Research: Space Physics*, *97*(A4), 4027–4039.

Angelopoulos, V., Coroniti, F., Kennel, C., Kivelson, M., Walker, R., Russell, C.,

... others (1996). Multipoint analysis of a bursty bulk flow event on april 11, 1985. *Journal of Geophysical Research: Space Physics*, *101*(A3), 4967–4989.

Angelopoulos, V., Kennel, C., Coroniti, F., Pellat, R., Kivelson, M., Walker, R., ... Gosling, J. (1994b). Statistical characteristics of bursty bulk flow events. *Journal of Geophysical Research: Space Physics*, *99*(A11), 21257–21280.

Angelopoulos, V., Kennel, C. F., Coroniti, F. V., Pellat, R., Kivelson, M. G., Walker, R. J., ... Gosling, J. T. (1994a). Statistical characteristics of bursty bulk flow events. *J. Geophys. Res.*, *99*, 21,257.

Angelopoulos, V., Phan, T., Larson, D., Mozer, F., Lin, R., Tsuruda, K., ... others (1997). Magnetotail flow bursts: association to global magnetospheric circulation, relationship to ionospheric activity and direct evidence for localization. *Geophysical research letters*, *24*(18), 2271–2274.

Angelopoulos, V., Runov, A., Zhou, X.-Z., Turner, D., Kiehas, S., Li, S.-S., & Shinohara, I. (2013). Electromagnetic energy conversion at reconnection fronts. *science*, *341*(6153), 1478–1482.

Asano, Y., Shinohara, I., Retinò, A., Daly, P., Kronberg, E., Takada, T., ... others (2010). Electron acceleration signatures in the magnetotail associated with substorms. *Journal of Geophysical Research: Space Physics*, *115*(A5).

Baker, D., Fritz, T., Wilken, B., Higbie, P., Kaye, S., Kivelson, M., ... others (1982). Observation and modeling of energetic particles at synchronous orbit on july 29, 1977. *Journal of Geophysical Research: Space Physics*, *87*(A8), 5917–5932.

Baumjohann, W., Paschmann, G., & Lühr, H. (1990). Characteristics of high-speed ion flows in the plasma sheet. *Journal of Geophysical Research: Space Physics*, *95*(A4), 3801–3809.

Birn, J., Hesse, M., & Schindler, K. (1996). MHD simulations of magnetotail dynamics. *J. Geophys. Res.*, *101*, 12,939.

Birn, J., Raeder, J., Wang, Y., Wolf, R., & Hesse, M. (2004). On the propagation of bubbles in the geomagnetic tail. In *Annales geophysicae* (Vol. 22, pp. 1773–1786).

Birn, J., Thomsen, M., Borovsky, J., Reeves, G., McComas, D., Belian, R., & Hesse, M. (1998). Substorm electron injections: Geosynchronous observations and test particle simulations. *Journal of Geophysical Research: Space Physics*, *103*(A5), 9235–9248.

Chen, Y., & Tóth, G. (2019). Gauss's law satisfying energy-conserving semi-implicit particle-in-cell method. *J. Comput. Phys.*, *386*, 632. doi: 10.1016/j.jcp.2019.02.032

Chen, Y., Tóth, G., Cassak, P., Jia, X., Gombosi, T. I., Slavin, J., ... Peng, B. (2017). Global three-dimensional simulation of earth's dayside reconnection using a two-way coupled magnetohydrodynamics with embedded particle-in-cell model: initial results. *J. Geophys. Res.*, *122*, 10318. doi: 10.1002/2017JA024186

Chen, Y., Tóth, G., Zhou, H., & Wang, X. (2023). Fleks: A flexible particle-in-cell code for multi-scale plasma simulations. *Computer Physics Communications*, *287*, 108714.

Chen, Y., Tóth, G., Hietala, H., Vines, S. K., Zou, Y., Nishimura, Y., ... Markidis, S. (2020). Magnetohydrodynamic with embedded particle-in-cell simulation of the geospace environment modeling dayside kinetic processes challenge event. *Earth and Space Science*, *7*(11), e2020EA001331. Retrieved from `https://agupubs.onlinelibrary.wiley.com/doi/abs/10.1029/2020EA001331` doi: https://doi.org/10.1029/2020EA001331

Chen, Y., Tóth, G., Jia, X., Slavin, J. A., Sun, W., Markidis, S., ... Raines, J. M. (2019). Studying dawn-dusk asymmetries of mercury's magnetotail using mhd-epic simulations. *Journal of Geophysical Research: Space Physics*, *124*(11), 8954-8973.

Daldorff, L. K. S., Tóth, G., Gombosi, T. I., Lapenta, G., Amaya, J., Markidis, S., & Brackbill, J. U. (2014). Two-way coupling of a global Hall magnetohydrodynamics model with a local implicit Particle-in-Cell model. *J. Comput. Phys.*, *268*, 236. doi: 10.1016/j.jcp.2014.03.009

Daughton, W., Roytershteyn, V., Karimabadi, H., Yin, L., Albright, B., Bergen, B., & Bowers, K. (2011). Role of electron physics in the development of turbulent magnetic reconnection in collisionless plasmas. *Nature Physics*, *7*(7), 539–542.

Eastwood, J., Goldman, M., Hietala, H., Newman, D., Mistry, R., & Lapenta, G. (2015). Ion reflection and acceleration near magnetotail dipolarization fronts associated with magnetic reconnection. *Journal of Geophysical Research: Space Physics*, *120*(1), 511–525.

Fu, H. S., Khotyaintsev, Y. V., André, M., & Vaivads, A. (2011). Fermi and betatron acceleration of suprathermal electrons behind dipolarization fronts. *Geophysical Research Letters*, *38*(16).

Fu, H. S., Khotyaintsev, Y. V., Vaivads, A., André, M., & Huang, S. (2012). Electric structure of dipolarization front at sub-proton scale. *Geophysical Research Letters*, *39*(6).

Gabrielse, C., Angelopoulos, V., Runov, A., & Turner, D. L. (2014). Statistical characteristics of particle injections throughout the equatorial magnetotail. *Journal of Geophysical Research: Space Physics*, *119*(4), 2512–2535.

Ge, Y., Raeder, J., Angelopoulos, V., Gilson, M., & Runov, A. (2011). Interaction of dipolarization fronts within multiple bursty bulk flows in global mhd simulations of a substorm on 27 february 2009. *Journal of Geophysical Research: Space Physics*, *116*(A5).

Gombosi, T. I., Chen, Y., Glocer, A., Huang, Z., Jia, X., Liemohn, M. W., ... others (2021). What sustained multi-disciplinary research can achieve: The space weather modeling framework. *Journal of Space Weather and Space Climate*, *11*, 42.

Henderson, M., Reeves, G., & Murphree, J. (1998). Are north-south aligned auroral structures an ionospheric manifestation of bursty bulk flows? *Geophysical Research Letters*, *25*(19), 3737–3740.

Hoshino, M. (2005). Electron surfing acceleration in magnetic reconnection. *Journal of Geophysical Research: Space Physics*, *110*(A10).

Huang, S., Fu, H., Yuan, Z., Zhou, M., Fu, S., Deng, X., ... others (2015). Electromagnetic energy conversion at dipolarization fronts: Multispacecraft results. *Journal of Geophysical Research: Space Physics*, *120*(6), 4496–4502.

Lapenta, G., Markidis, S., Divin, A., Goldman, M., & Newman, D. (2010). Scales of guide field reconnection at the hydrogen mass ratio. *Physics of Plasmas*, *17*(8), 082106.

Li, C., Jia, X., Chen, Y., Toth, G., Zhou, H., Slavin, J. A., ... Poh, G. (2023). Global hall mhd simulations of mercury's magnetopause dynamics and ftes under different solar wind and imf conditions. *Journal of Geophysical Research: Space Physics*, *128*(5), e2022JA031206. Retrieved from `https://agupubs.onlinelibrary.wiley.com/doi/abs/10.1029/2022JA031206` (e2022JA031206 2022JA031206) doi: https://doi.org/10.1029/2022JA031206

Liu, C., Fu, H., Xu, Y., Cao, J., & Liu, W. (2017). Explaining the rolling-pin distribution of suprathermal electrons behind dipolarization fronts. *Geophysical Research Letters*, *44*(13), 6492–6499.

Liu, Y.-H., Birn, J., Daughton, W., Hesse, M., & Schindler, K. (2014). Onset of reconnection in the near magnetotail: Pic simulations. *Journal of Geophysical Research: Space Physics*, *119*(12), 9773–9789.

Lu, S., Angelopoulos, V., & Fu, H. (2016). Suprathermal particle energization in dipolarization fronts: Particle-in-cell simulations. *Journal of Geophysical Research: Space Physics*, *121*(10), 9483–9500.

Lyon, J., Fedder, J., & Mobarry, C. (2004). The Lyon-Fedder-Mobarry (LFM) global

MHD magnetospheric simulation code. *J. Atmos. Sol-Terr. Phys.*, *66*, 1333.

Ma, Y., Russell, C. T., Toth, G., Chen, Y., Nagy, A. F., Harada, Y., ... others (2018). Reconnection in the martian magnetotail: Hall-mhd with embedded particle-in-cell simulations. *Journal of Geophysical Research: Space Physics*, *123*(5), 3742–3763.

Nakamura, R., Baumjohann, W., Klecker, B., Bogdanova, Y., Balogh, A., Rème, H., ... others (2002). Motion of the dipolarization front during a flow burst event observed by cluster. *Geophysical research letters*, *29*(20), 3–1.

Nakamura, R., Retinò, A., Baumjohann, W., Volwerk, M., Erkaev, N., Klecker, B., ... Khotyaintsev, Y. (2009). Evolution of dipolarization in the near-earth current sheet induced by earthward rapid flux transport. In *Annales geophysicae* (Vol. 27, pp. 1743–1754).

Øieroset, M., Lin, R., Phan, T., Larson, D., & Bale, S. (2002). Evidence for electron acceleration up to 300 k e v in the magnetic reconnection diffusion region of earth's magnetotail. *Physical Review Letters*, *89*(19), 195001.

Pollock, C., Moore, T., Jacques, A., Burch, J., Gliese, U., Saito, Y., ... others (2016). Fast plasma investigation for magnetospheric multiscale. *Space Science Reviews*, *199*, 331–406.

Powell, K., Roe, P., Linde, T., Gombosi, T., & De Zeeuw, D. L. (1999). A solution-adaptive upwind scheme for ideal magnetohydrodynamics. *J. Comput. Phys.*, *154*, 284-309. doi: 10.1006/jcph.1999.6299

Pritchett, P. (2006). Relativistic electron production during driven magnetic reconnection. *Geophysical research letters*, *33*(13).

Raeder, J., Larson, D., Li, W., Kepko, E. L., & Fuller-Rowell, T. (2008). Openggcm simulations for the themis mission. *Space Science Reviews*, *141*, 535–555.

Ridley, A., Gombosi, T., & Dezeeuw, D. (2004, February). Ionospheric control of the magnetosphere: conductance. *Annales Geophysicae*, *22*, 567-584. doi: 10.5194/angeo-22-567-2004

Runov, A., Angelopoulos, V., Gabrielse, C., Liu, J., Turner, D., & Zhou, X.-Z. (2015). Average thermodynamic and spectral properties of plasma in and around dipolarizing flux bundles. *Journal of Geophysical Research: Space Physics*, *120*(6), 4369–4383.

Runov, A., Angelopoulos, V., Sitnov, M., Sergeev, V., Bonnell, J., McFadden, J., ... Auster, U. (2009). Themis observations of an earthward-propagating dipolarization front. *Geophysical Research Letters*, *36*(14).

Runov, A., Angelopoulos, V., & Zhou, X.-Z. (2012). Multipoint observations of dipolarization front formation by magnetotail reconnection. *Journal of Geophysical Research: Space Physics*, *117*(A5).

Sun, W., Turner, D. L., Zhang, Q., Wang, S., Egedal, J., Leonard, T., ... others (2022). Properties and acceleration mechanisms of electrons up to 200 kev associated with a flux rope pair and reconnection x-lines around it in earth's plasma sheet. *Journal of Geophysical Research: Space Physics*, *127*(12), e2022JA030721.

Toffoletto, F., Sazykin, S., Spiro, R., & Wolf, R. (2003). Inner magnetospheric modeling with the Rice Convection Model. *Space Sci. Rev.*, *107*, 175-196. doi: 10.1023/A:1025532008047

Tóth, G., Chen, Y., Gombosi, T. I., Cassak, P., Markidis, S., & Peng, B. (2017). Scaling the ion inertial length and its implications for modeling reconnection in global simulations. *J. Geophys. Res.*, *122*, 10336. doi: 10.1002/2017JA024189

Tóth, G., Jia, X., Markidis, S., Peng, B., Chen, Y., Daldorff, L., ... Dorelli, J. (2016). Extended magnetohydrodynamics with embedded particle-in-cell simulation of ganymede's magnetosphere. *J. Geophys. Res.*, *121*. doi: 10.1002/2015JA021997

Tóth, G., Ma, Y. J., & Gombosi, T. I. (2008). Hall magnetohydrodynamics on block adaptive grids. *J. Comput. Phys.*, *227*, 6967-6984. doi: 10.1016/j.jcp.2008.04

.010

Tóth, G., van der Holst, B., Sokolov, I. V., Zeeuw, D. L. D., Gombosi, T. I., Fang, F., ... Opher, M. (2012). Adaptive numerical algorithms in space weather modeling. *J. Comput. Phys.*, *231*, 870–903. doi: 10.1016/j.jcp.2011.02.006

Wang, X., Chen, Y., & Tóth, G. (2022a). Global magnetohydrodynamic magnetosphere simulation with an adaptively embedded particle-in-cell model. *Journal of Geophysical Research: Space Physics*, *127*(8), e2021JA030091.

Wang, X., Chen, Y., & Tóth, G. (2022b). Simulation of magnetospheric sawtooth oscillations: The role of kinetic reconnection in the magnetotail. *Geophysical Research Letters*, *49*(15), e2022GL099638.

Wiltberger, M., Merkin, V., Lyon, J., & Ohtani, S. (2015). High-resolution global magnetohydrodynamic simulation of bursty bulk flows. *Journal of Geophysical Research: Space Physics*, *120*(6), 4555–4566.

Wiltberger, M., Pulkkinen, T., Lyon, J., & Goodrich, C. (2000). MHD simulation of the magnetotail during the December 10, 1996, substorm. *J. Geophys. Res.*, *105*, 27,649.

Wolf, R. A., Harel, M., Spiro, R. W., Voigt, G., Reiff, P. H., & Chen, C. K. (1982). Computer simulation of inner magnetospheric dynamics for the magnetic storm of July 29, 1977. *J. Geophys. Res.*, *87*, 5949-5962. doi: 10.1029/JA087iA08p05949

Xu, Y., Fu, H., Norgren, C., Toledo-Redondo, S., Liu, C., & Dong, X. (2019). Ionospheric cold ions detected by mms behind dipolarization fronts. *Geophysical Research Letters*, *46*(14), 7883–7892.

Zhou, H., Tóth, G., Jia, X., & Chen, Y. (2020). Reconnection-driven dynamics at ganymede's upstream magnetosphere: 3-d global hall mhd and mhd-epic simulations. *Journal of Geophysical Research: Space Physics*, *125*(8), e2020JA028162.

Zhou, H., Tóth, G., Jia, X., Chen, Y., & Markidis, S. (2019). Embedded kinetic simulation of ganymede's magnetosphere: Improvements and inferences. *Journal of Geophysical Research: Space Physics*, *124*(7), 5441–5460.

Zhou, X.-Z., Angelopoulos, V., Sergeev, V., & Runov, A. (2010). Accelerated ions ahead of earthward propagating dipolarization fronts. *Journal of Geophysical Research: Space Physics*, *115*(A5).

Zhou, X.-Z., Angelopoulos, V., Sergeev, V., & Runov, A. (2011). On the nature of precursor flows upstream of advancing dipolarization fronts. *Journal of Geophysical Research: Space Physics*, *116*(A3).

Zhou, X.-Z., Pan, D.-X., Angelopoulos, V., Liu, J., Runov, A., Li, S.-S., ... Fu, S.-Y. (2015). Ion acceleration and reflection on magnetotail antidipolarization fronts. *Geophysical Research Letters*, *42*(21), 9166–9175.

Zhou, X.-Z., Xu, Y., Runov, A., Liu, J., Artemyev, A. V., Angelopoulos, V., ... Zong, Q.-G. (2019). On the origin of perpendicular ion anisotropy inside dipolarizing flux bundles. *Journal of Geophysical Research: Space Physics*, *124*(6), 4009–4021.